energies

MDPI

Article

Effect of Roof Cooling and Air Curtain Gates on Thermal and Wind Conditions in Stadiums for Hot Climates

Fangliang Zhong [1,*], Hassam Nasarullah Chaudhry [2] and John Kaiser Calautit [1]

[1] Department of Architecture and Built Environment, Faculty of Engineering, University of Nottingham, Nottingham NG7 2RD, UK; john.calautit1@nottingham.ac.uk
[2] School of Energy, Geoscience, Infrastructure and Society, Heriot-Watt University Dubai Campus, Heriot-Watt University, Dubai Knowledge Park, Dubai P.O. Box 38103, United Arab Emirates; h.n.chaudhry@hw.ac.uk
* Correspondence: Fangliang.Zhong@outlook.com

Abstract: To host the 2022 FIFA World Cup, Qatar is facing the greatest challenge in balancing the energy consumptions for cooling the stadiums and the thermal comfort for both players and spectators. Previous studies have not considered using a combined configuration of air curtain and roof cooling supply slot in stadiums to prevent the infiltration of outside hot air and reduce the cooling system's energy consumption. This paper presents a Computational Fluid Dynamics (CFD) study of thermal and wind modeling around a baseline stadium and simulates the cooling scenarios of air curtains and roof cooling along with the energy consumption estimations for the World Cup matches using Building Energy Simulation (BES). Sensitivity analysis of different supply speeds and supply temperatures of air curtain gates and roof cooling was carried out, and the results showed that scenario six, which provides supply air of 25 m/s and 20 m/s at the roof and air curtain gates with a supply temperature of 10 °C, demonstrates optimal thermal performances on both the spectator tiers and the pitch. Compared with the baseline stadium performance, the average reductions in temperature on the pitch and spectator tiers under scenario six could reach 15 °C and 14.6 °C. The reductions in the Predicted Percentage of Dissatisfied values for the upper and lower tiers as well as the pitch were 63%, 74%, and 78%. In terms of the estimated energy consumptions, scenario six would consume electric energy per match at a rate of 25.5 MWh compared with 22.8 MWh for one of the stadiums in the 2010 South Africa World Cup and 42.0 MWh for the 2006 Germany World Cup. Future research is recommended to explore the influence of supply angle on air curtain gates and roof cooling supply slots' performances.

Keywords: computational fluid dynamics; stadium cooling; air curtain; building energy simulation; thermal comfort; hot climates

Citation: Zhong, F.; Chaudhry, H.N.; Calautit, J.K. Effect of Roof Cooling and Air Curtain Gates on Thermal and Wind Conditions in Stadiums for Hot Climates. *Energies* **2021**, *14*, 3941. https://doi.org/10.3390/en14133941

Academic Editor: Paweł Ocłoń

Received: 3 June 2021
Accepted: 27 June 2021
Published: 1 July 2021

1. Introduction and Literature Review

Hosting the twenty-second edition of the FIFA World Cup in 2022 will be a unique opportunity to create a positive, sustainable legacy for Qatar [1], but the country faces the greatest challenges in conforming to the Green Goal vision launched by FIFA in 2006 [2]. As one of the objectives of the Green Goal policy [2], Qatar must host a net-zero carbon dioxide emission World Cup, a world first. Qatar is in the hot climate region, where cooling can account for a significant portion (up to 36%) of the region's total electricity consumption [3]. While FIFA's comfort temperature range is 20–25.5 °C for the spectator terraces or zones [4]. Thus, balancing the stadiums' cooling energy consumptions and the aero-thermal comfort for both players and spectators becomes a great challenge for Qatar. For the first time, the 2022 tournament will be held in the winter from November to December [5] to avoid the extreme summer heat. However, it is still challenging to maintain the temperature at spectator tiers within the threshold range and to provide comfortable spaces for both the spectators and players at the expense of low energy consumptions since the outdoor design temperature can still be up to 34 °C [6]. Therefore, the country should employ

energy-efficient cooling strategies [7,8] or low energy/passive cooling techniques [9,10] to minimize the significant energy usage for cooling the stadia. Moreover, computational fluid dynamics (CFD) tools are powerful in investigating the temperature distributions and wind flow conditions around and within building structures [11,12].

Most of the existing studies on stadiums have not paid much attention to evaluating the thermal environment in stadiums and the influence on the comfort levels of the spectators and players. Furthermore, there are also limited studies on developing and integrating cooling technologies into stadiums situated in these regions. Many of the works focused on evaluating the wind environment within and around the stadium and its influence on airflow distribution and wind comfort. In most cases, CFD modeling validated with experiments was employed in these studies. For example, a stadium in the Netherlands was simulated by [13] using CFD, which was validated with full-scale field tests. The study's focus was to evaluate the natural ventilation occurring through the openings of the stadium, which includes the roof, side gates, and openings between the stands and the roof. The work highlighted the capabilities of the method to model the complex geometry of the stadium and the importance of taking into account the surrounding urban environment. The modeling was based on steady Reynolds-averaged Navier–Stokes equations (RANS), which generally showed good agreement with the measurements, but the authors noted its inability to model the inherently transient effects. A thermal simulation was also carried out with fixed surface temperature, but the stadia thermal distribution was not adequately discussed. The study noted the importance of thermal effects on ventilation rates.

Using the same modeling approach, van Hooff and Blocken [14] evaluated the impact of the urban environment and the wind direction on the stadium's natural ventilation rates in the Netherlands. Similarly, the model was validated with full-scale wind measurements, which are detailed in [15]. A good agreement was obtained between the two methods. Unlike their previous work, they did not take into account the thermal effects and buoyancy-driven flows. The study highlighted the importance of modeling the stadium's buildings, particularly when it is naturally ventilated. It was observed that an overestimation of the air change rate per hour of up to 96% could occur when not including the surrounding urban environment. Using the same case study stadium, the study [15] carried out full-scale measurements to evaluate the indoor environment conditions, focusing on the air temperature, natural ventilation, and CO_2 concentration when the stadium was used during concerts. The study highlighted the influence of the sky's irradiation, the fabric, and the heat generated by the spectators on the indoor air temperature. The spectators also significantly influenced the humidity and CO_2 concentration levels within the stadium.

Similarly, the work of Sofotasiou [16] evaluated the wind environment and comfort in a semi-enclosed stadium using CFD modeling but employed scaled wind tunnel testing to validate the simulation results. The study also employed the response surface methodology (RSM) approach to optimize the stadium roof geometry. The work highlighted the influence of the design changes on both the spectators' tiers and the center of the pitch. Using the same case study stadium in the Netherlands, the work [17] employed the dynamic thermal modeling tool Ecotect to estimate the cooling load required per game to provide comfort conditions in the spectator tiers, playing field, and facilities. The results showed that the cooling load for each match could range between 47–115 MWh depending on the outdoor conditions and set cooling operation.

Several works evaluated the thermal environment inside stadiums and cooling strategies for stadiums. Losi et al. [18] used the CFD tool OpenFoam to model the thermal comfort in a stadium situated in a hot and humid climate. The stadium was assumed to be air-conditioned and employed air nozzles in the spectator tiers. The study simulated different climatic conditions and air conditioning system duty cycles. The thermal comfort was evaluated based on the predicted mean vote method. Due to the lack of experimental data, the models' predictions were not validated in their work. The study of Ghani et al. [19] also evaluated the performance of an airconditioned stadium located in a hot and humid climate but focused on the football pitch area. The work employed direct numerical

simulation and ENVI-met climate model to simulate the heat transfer between the pitch and the microclimate. The model was validated with field experiment measurements, and good agreement was observed except for peak temperature periods. While the work of [20] focused on the thermal environment in the spectator tiers in stadiums in hot climates. The study employed CFD to evaluate the air velocity and temperature distribution around the spectators to optimize thermal comfort. Different cooling strategies and operations, radiant cooling, and air-jet locations were evaluated. The work also highlighted the potential impact of the seating material on the spectator's comfort levels.

More recently, the work carried out by Zhong, Calautit, and Hughes [21] also explored the influence of the positioning of the air cooling jets on the ventilation and thermal performance of stadiums in hot climates but considered the entire stadium bowl. The study attempted to address the issue observed by [16] regarding the uneven airflow velocity and temperature distribution around the spectators' tiers and the center of the pitch. The work evaluated several cooling jet configurations and concluded that adding vertical and horizontal cooling jets at the spectator tiers and arrays of jets around the pitch performed the best. The results highlighted that the biggest challenge when cooling a semi-enclosed stadium is the roof opening where external hot air enters the stadium and at the same time exhaust the cooling supply air out. Another challenge is the hot air entering the stadium's gates, which resulted in higher pitch temperature, which is a concern for the football players during the match. A potential solution to this is the use of cooling strategies such as air curtains [22,23] which can project continuous airstream across the envelope's opening, limiting or preventing unconditioned air from entering the indoor conditioned spaces. While, at the same time, not limiting or interrupting the access of the thousands of people between the two different environments.

Aside from building entrances, air curtains are used for diverse applications such as refrigerated storages [24,25], tunnels [26], and train stations [27]. Many studies [28,29] have evaluated air curtain airflow characteristics and performance. An infiltration model was developed by [29] for doors with air curtains. While the study by [30] developed a CFD model of air curtains validated by experimental data and compared with the simplified model developed by [29]. A parametric analysis was carried out by [31] to enhance the performance of air curtains in terms of reducing and infiltration. The study employed scaled experiments and CFD modeling to evaluate the impact of airflow supply speed and angle and people below the jets. Based on the review of previous works, the analysis of air curtain performance at the entrances of stadiums has been limited. The effect of roof cooling strategy by adding air-jet supply slots at the roof on semi-open stadiums' wind and thermal conditions has not yet been fully explored.

The aim of this work is to evaluate the aero-thermal conditions in stadiums equipped with roof cooling air jet slots and air curtain gates in hot climates and to explore the influence of the supply velocity and the supply temperature of roof cooling supply slots and air curtain on the cooling performance of stadiums in hot climates. Full-scale CFD simulations were implemented in this study. The stadium model was developed based on [15], which was also used to validate the modeling approach. The CFD modeling method of air curtain supply in this present work was validated by previous work results [30]. In order to model the thermal conditions with consideration of the effect of solar irradiance on the interior and exterior surfaces, de-coupled CFD simulations, including the turbulence, energy, and radiation models, were conducted for the baseline stadium without air curtain gates and roof cooling to evaluate the surface radiative heat flux. Six scenarios of different airflow supply speeds and supply temperatures for roof cooling supply and air curtains were proposed and compared based on the indoor environment conditions obtained from the simulation results. The thermal comfort levels in the spectator zone and pitch were assessed and compared among these scenarios. The baseline thermal performance of the stadium was also evaluated to determine the cooling effect of the air curtains and roof cooling on the stadium. Furthermore, the energy consumption estimation for each cooling scenario was performed using the building energy simulation software EnergyPlus.

2. Methods

In this research, a CFD stadium model was created in ANSYS Fluent 18 based on the works of van Hooff and Blocken [13,14] and the wind velocity measurements from van Hooff and Blocken [15] was used to validate the modeling approach. The air curtains were also modeled in Fluent 18 and verified using the previous work [30]. The solar irradiance, an important parameter affecting the internal and external surface temperatures, was also simulated. However, it was assessed in a set of separate simulations from the stadium's evaluation equipped with air curtains and roof cooling to reduce the computational cost and time. The predicted radiative surface heat flux on the internal and external surfaces were used as boundary conditions for the simulation of the cooling strategies in the stadium. The indoor environment of the stadium was assessed under a prevailing wind angle of 292.5° in Doha. Different scenarios of air curtains and roof cooling were simulated. This section describes the stadium geometry and domain dimensions and the cell sizes for the computational grid. The method and results of a grid-independent study are also presented. The Fluent setup for radiation analysis is explained as well. In addition, the boundary conditions and the Fluent solver settings for the simulations are given. Moreover, the modeling method and parameter settings of EnergyPlus simulations for the energy estimations of the World Cup matches were included.

2.1. Stadium Geometry and Computational Domain

The three-dimensional geometry developed (Figure 1b) was based on a case study stadium in Amsterdam (Figure 1a) [13]. Based on the suggestion of previous work [14,32], the neighboring buildings were also modeled full scale in the computational domain. The stadium model's length, width, and height were 226 m, 190 m, and 72 m, respectively (Figure 2). The interior volume was 1.2 mil m^3. For the purpose of ventilating the stadium, the roof (Figure 2) serves as the largest opening (110 m × 40 m), and the four gates of the stadium are the second-largest (Figure 2) [13]. Each gate has a dimension of 6.2 m × 6.7 m ($W_g \times H_g$) and is labeled by an arrow in Figure 2. The pitch is located 2.1 m above the stadium's deck. The domain's length, width, and height are 1896 m, 1461 m, and 432 m, respectively. The distance between the stadium and inlet, outlet, side, and top walls was set based on the guidelines and suggestions of [33–37] (Figure 1c,d). It should be noted that the distance between the stadium leeward surface and the pressure outlet was reduced from fifteen times the height of the stadium (15H) to ten times the height of the stadium (10H) in order to reduce the computational cost and time. However, it was ensured that it had minimal impact on the simulations, and the reverse flow issue at the pressure outlet was not observed during the calculations.

2.2. Details of CFD Mesh

The accuracy and time cost of CFD simulations are substantially influenced by the quality of the computational mesh [38]. For CFD models which simulate the indoor and outdoor flow simultaneously in the same computational domain, the significant geometrical length scale differences between the urban environment and the stadium structure will lead to a large domain with high-resolution mesh [13]. Thus, local control over the entire mesh was employed to enhance the quality of the mesh. A mesh with 9.3 mil tetrahedron elements was generated and used for the analysis. The cell sizes of the stadium, surrounding buildings, and the remaining domain were set to 1 m, 2.5 m, and 8 m, respectively. The mesh was selected based on a grid independence analysis which simulated two additional mesh sizes of 6.5 million and 12.3 million elements. The cell sizes of the stadium and surrounding buildings were adjusted to 1.5 m and 3 m for the coarse mesh and 0.8 m and 2 m for the fine mesh. The wind velocity and temperature, which were the main variables in this study, were recorded by 7 measurement points in the stadium, and 9 measurement points on the pitch (Figure 3). The absolute mean errors of the measured variables between the two meshes are calculated as follows:

$$\delta_1 = \frac{1}{16}\sum_{i=1}^{16}\left|\frac{v_{i-coarse} - v_{i-medium}}{v_{i-coarse}}\right| \times 100\% \quad (1)$$

$$\delta_2 = \frac{1}{16}\sum_{i=1}^{16}\left|\frac{v_{i-medium} - v_{i-fine}}{v_{i-medium}}\right| \times 100\% \quad (2)$$

$$\theta_1 = \frac{1}{16}\sum_{i=1}^{16}\left|\frac{T_{i-coarse} - T_{i-medium}}{T_{i-coarse}}\right| \times 100\% \quad (3)$$

$$\theta_2 = \frac{1}{16}\sum_{i=1}^{16}\left|\frac{T_{i-medium} - T_{i-fine}}{T_{i-medium}}\right| \times 100\% \quad (4)$$

where $v_{i-coarse}$, $v_{i-medium}$ and v_{i-fine} represent the wind velocities at measurement point i for the different mesh sizes; $T_{i-coarse}$, $T_{i-medium}$ and T_{i-fine} represent the air temperature at measurement point i for the different mesh sizes. The wind velocity results showed that the mean error was 58.38% between the coarse and medium mesh and 29.66% between the medium and fine mesh. The error was 6.47% between the coarse and medium mesh and 4.99% between the medium and fine mesh for the temperature results. Therefore, the medium mesh was selected due to its better accuracy in predicting simulation results and relatively less computational cost.

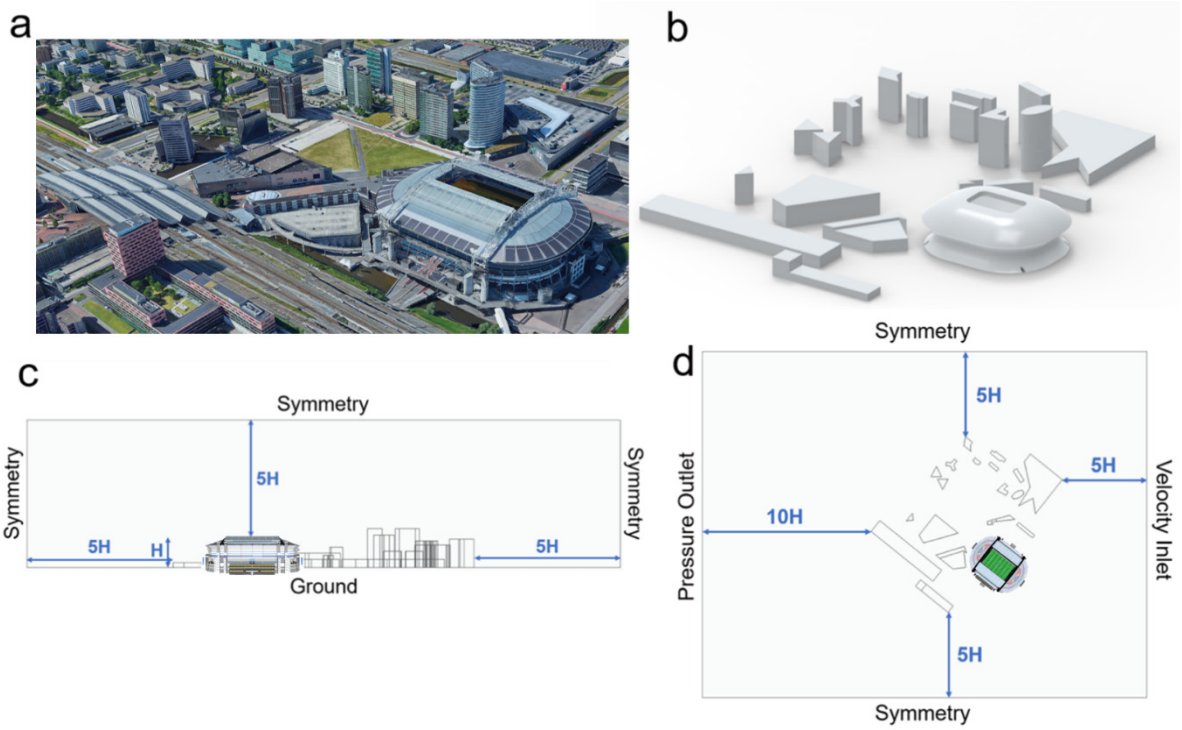

Figure 1. (**a**) Semi-enclosed stadium with neighboring buildings within 300 m from the stadium. (**b**) Three-dimensional CAD geometry model of the stadium. (**c**) Vertical cross-section view of the computational domain. (**d**) Horizontal cross-section view of the computational domain.

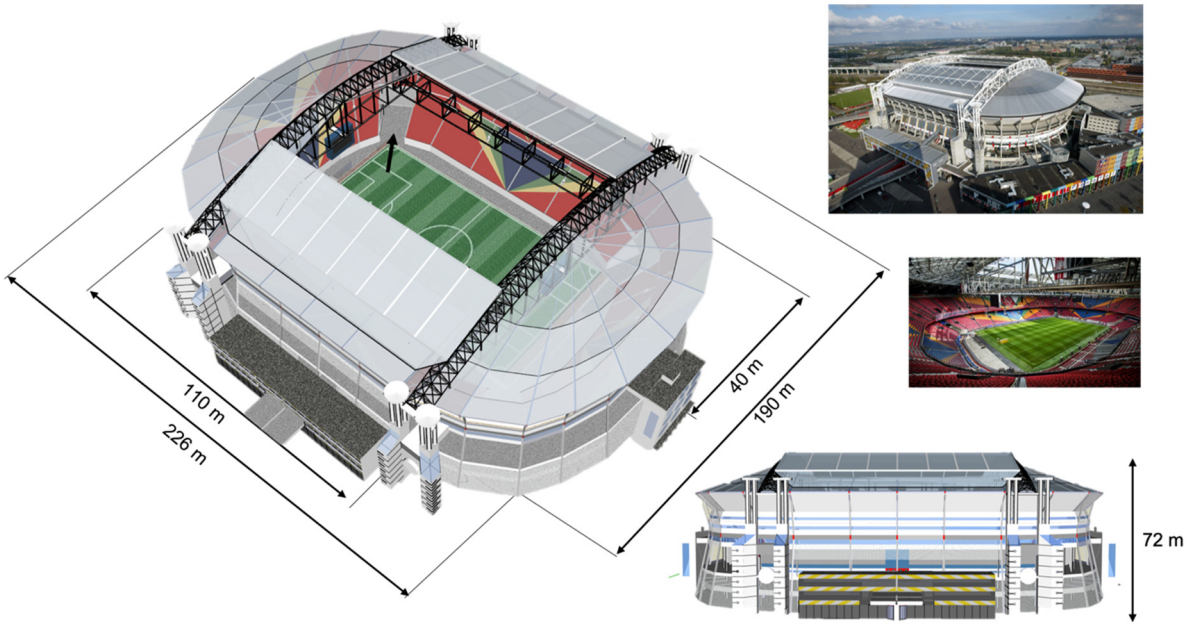

Figure 2. The semi-enclosed stadium main dimensions.

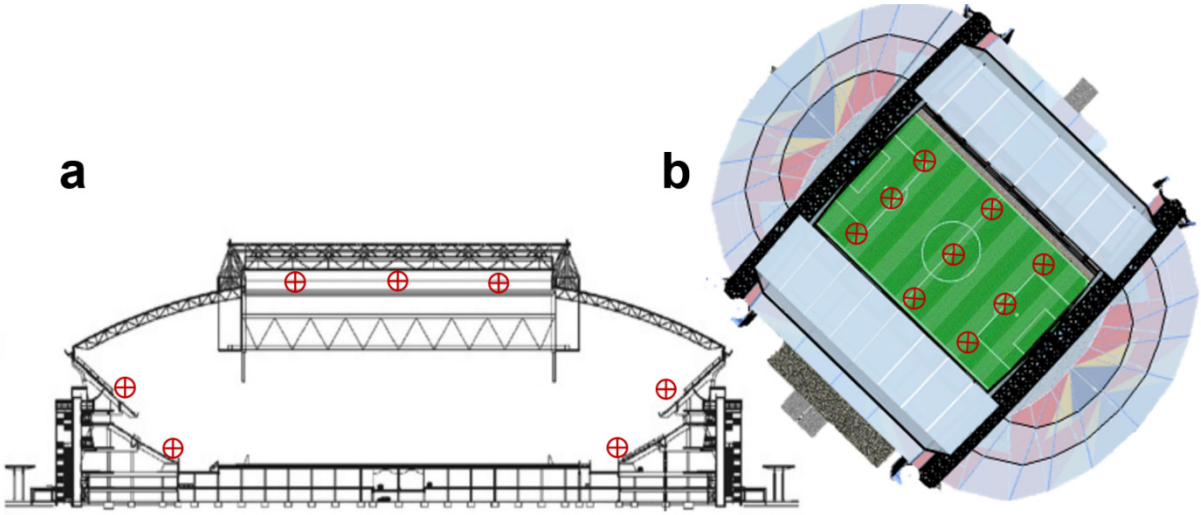

Figure 3. Grid independence analysis: (**a**) Measurement points on the cross-section of the stadium. (**b**) Measurement points on the pitch.

2.3. Solar Radiation Analysis Setup

A separate solar radiation analysis, apart from the simulations of thermal and wind conditions for cooling scenarios and the baseline stadium, was conducted to simulate the entire model under the Doha solar irradiance data and to predict the heat fluxes on the external and internal surfaces. This will reduce the gap between the actual conditions of the stadium and the CFD simulation results. The radiative heat fluxes on these surfaces were simulated under the proposed World Cup match kick-off times on the event opening day, i.e., 1 PM, 4 PM, 7 PM, and 10 PM (Doha time) [39]. The simulations employed the Discrete Ordinates (DO) model with the solar ray tracing method [38]. The solar irradiation method used to calculate the solar load under each kick-off time was based on fair weather conditions [38]. The sunshine factor was set up as 0.3, and the resultant direct normal irradiance and diffuse horizontal irradiance at 13:00 were 288.5 W/m^2 and 60.6 W/m^2. These values of solar irradiances were compared with the limited measurements of solar irradiances in Doha and verified to be within the acceptable range [40].

2.4. Boundary Conditions

The validation for the modeling of the stadium and urban environment was performed under the wind direction of φ = 350°. The prevailing weather conditions for November and December, the World Cup months, in Doha were used to set the inlet boundary conditions in the simulations of the stadium without and with air curtains and roof cooling. The model simulated the prevailing wind direction during the event period in Doha is west-north-west [41] or φ = 292.5° (Figure 4a,b). The boundary conditions of the domain, stadium, and neighboring buildings are illustrated in Figure 5.

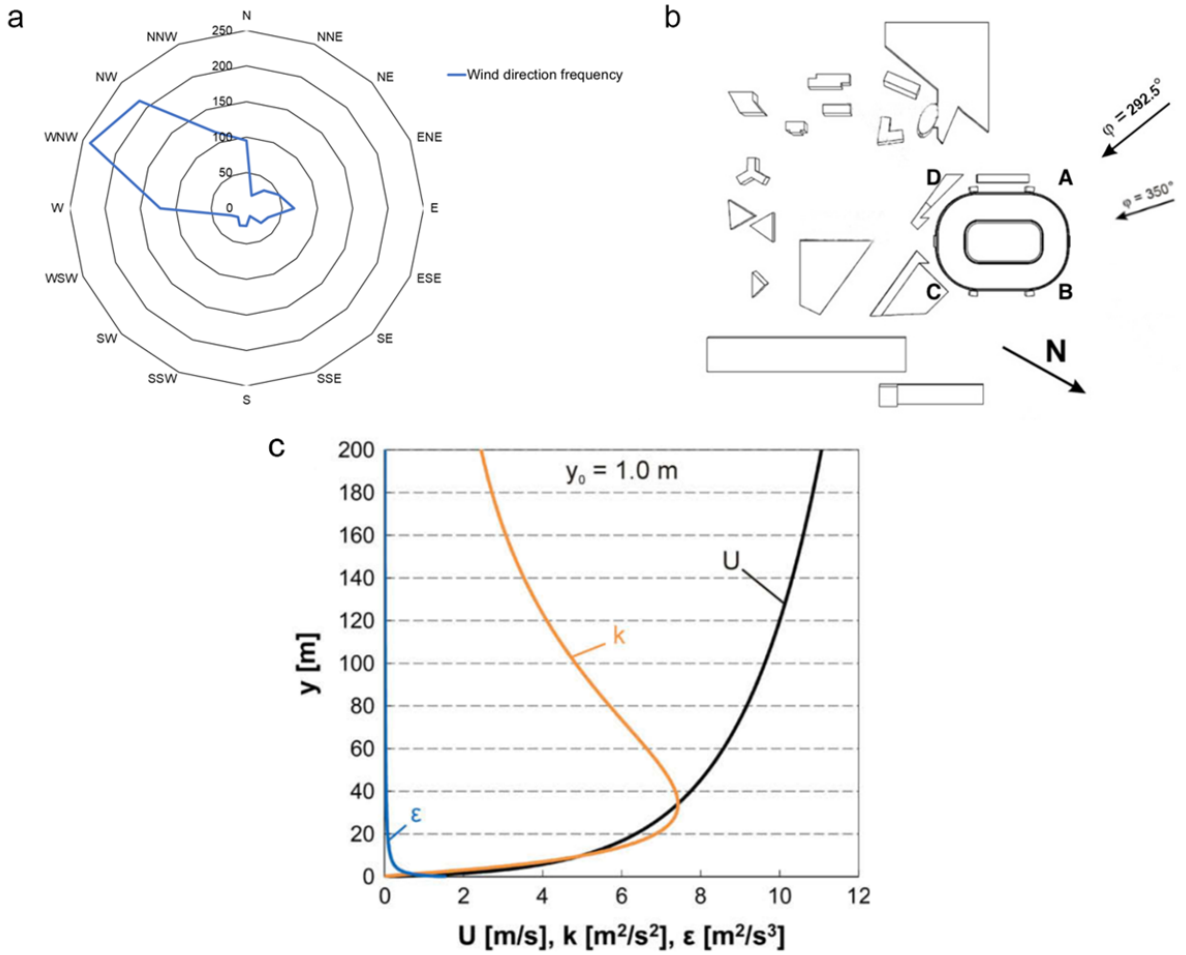

Figure 4. (**a**) The frequency of wind direction during the match period. (**b**) The wind direction in the simulation (where A–D are the four gates of the stadium). (**c**) Approach wind velocity profiles, turbulence kinetic energy, and dissipation rate [14].

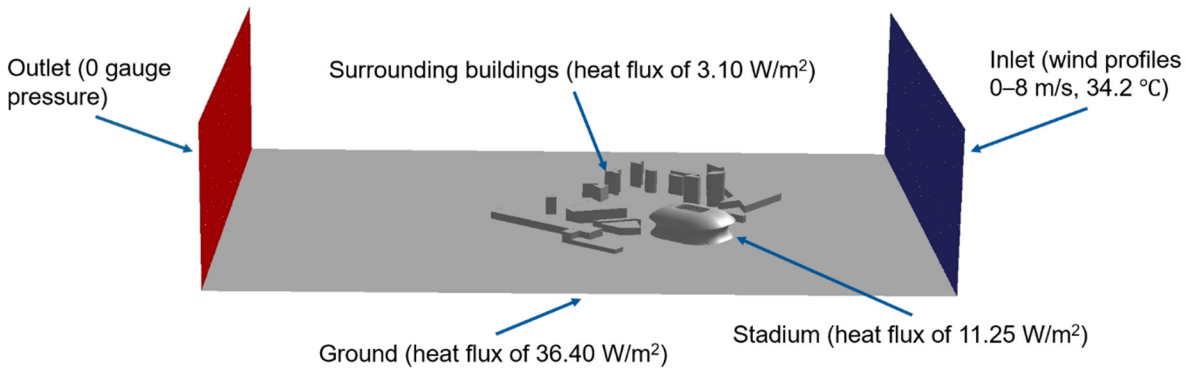

Figure 5. Boundary conditions as defined for the CFD model.

The highest outdoor design temperature for the event months [6], 34.2 °C, was used as the inlet air temperature. The wind profiles at the inlet for both wind directions were created according to [42]. The pressure outlet was set as atmospheric pressure. The sidewalls of the domain were set to symmetrical. The turbulent kinetic energy and dissipation rate profiles in Figure 4c were also set at the inlet. The wall roughness was set based on the recommendations of [43,44]. According to the results of solar radiation simulations, the predicted heat fluxes were used for the ground, stadium, and neighboring building surfaces. The soil was set as the material used for the ground, and concrete was set as the material for the stadium. The air curtains and roof cooling supply slots were modeled as velocity inlets based on each cooling scenario. The details of the boundary conditions were provided in Table 1. The supply velocity and temperature, as well as the position of each air curtain or roof cooling supply slot, are presented in Table 2.

Table 1. Boundary conditions for the CFD simulations.

CFD Boundary Conditions	
Domain inlet	Velocity-inlet with a wind profile of aerodynamic roughness length y0 = 1 m; inflow temperature of 34.2 °C.
Domain Outlet	Pressure-outlet with gauge pressure of 0 Pa; backflow temperature of 34.2 °C.
Ground (wall)	k_s = 0.59, m C_s = 0.5; heat flux of 36.40 W/m^2; material is set up as soil (r = 1400 kg/m^3; Cp = 1480 J/(kgK); k = 0.75 W/(mK) [45].
Stadium (wall)	k_s = 0 m, C_s = 0.5; heat flux of 11.25 W/m^2; material is set up as concrete (r = 2400 kg/m^3; Cp = 880 J/(kgK); k = 0.3 W/(mK) [45].
Surrounding buildings (wall)	k_s = 0 m, C_s = 0.5; heat flux of 3.10 W/m^2; material is set up as concrete (r = 2400 kg/m^3; Cp = 880 J/(kgK); k = 0.3 W/(mK) [45].
Air curtain and roof cooling supply	Velocity inlet with constant speeds; temperatures of 20 °C, 15 °C, and 10 °C.

Table 2. Air curtain and roof cooling scenarios proposed in sensitivity studies.

Scenario 1	**Position**	**Supply Velocity (m/s)**	**Supply Temperature (°C)**
Roof cooling	Roof	20	20
Air curtain 1	Gate A	10	20
Air curtain 2	Gate B	10	20
Air curtain 3	Gate C	10	20
Air curtain 4	Gate D	10	20
Scenario 2	**Position**	**Supply Velocity (m/s)**	**Supply Temperature (°C)**
Roof cooling	Roof	25	20
Air curtain 1	Gate A	15	20
Air curtain 2	Gate B	15	20
Air curtain 3	Gate C	15	20
Air curtain 4	Gate D	15	20
Scenario 3	**Position**	**Supply Velocity (m/s)**	**Supply Temperature (°C)**
Roof cooling	Roof	30	20
Air curtain 1	Gate A	20	20
Air curtain 2	Gate B	20	20
Air curtain 3	Gate C	20	20
Air curtain 4	Gate D	20	20

Table 2. *Cont.*

Scenario 4	Position	Supply Velocity (m/s)	Supply Temperature (°C)
Roof cooling	Roof	25	20
Air curtain 1	Gate A	20	20
Air curtain 2	Gate B	20	20
Air curtain 3	Gate C	20	20
Air curtain 4	Gate D	20	20
Scenario 5	**Position**	**Supply Velocity (m/s)**	**Supply Temperature (°C)**
Roof cooling	Roof	25	15
Air curtain 1	Gate A	20	15
Air curtain 2	Gate B	20	15
Air curtain 3	Gate C	20	15
Air curtain 4	Gate D	20	15
Scenario 6	**Position**	**Supply Velocity (m/s)**	**Supply Temperature (°C)**
Roof cooling	Roof	25	10
Air curtain 1	Gate A	20	10
Air curtain 2	Gate B	20	10
Air curtain 3	Gate C	20	10
Air curtain 4	Gate D	20	10

2.5. CFD Solver Settings

The CFD simulations were based on the steady RANS equations with the realizable k-ε turbulence model, which can predict the wind flow conditions around structures more accurately, especially in simulating the wake regions near structures [46,47] compared to the standard model. The relevant variables, such as wind velocity, were monitored to manually control the end of the simulation. The parallel simulations were conducted on a workstation that included 2 × Intel Xeon E5-2670 2.60 GHz CPUs and 24 GB RAM. The solution was converged at 4000 iterations with residuals of 10^{-2} for continuity, 10^{-4} for x, y, and z velocities, 10^{-7} for energy, 10^{-4} for k, and 10^{-3} for epsilon. The computational time/simulation was around 18 h. Table 3 summarizes the details of solver settings.

Table 3. The Fluent solver settings used the in simulations.

Fluent Solver Settings	
Steady/transient simulation	Steady-state
Turbulence model	Realizable k-ε model with standard wall functions and full buoyancy effect
Solution method	Pressure-velocity coupling
Scheme	SIMPLE
Spatial discretization	Second-order discretization schemes
Under-relaxation factors	Default values
Convergence Criteria	None (Manually control to the end of calculation)

2.6. Building Energy Simulation (BES) Settings

Energy consumption estimation for each cooling scenario was performed in the widely used BES software, EnergyPlus version 9.3 [48]. EnergyPlus is a thermal load sizing and building energy simulation software that calculates heating and cooling loads for each thermal zone using the ASHRAE heat balance method [22] for HVAC system sizing and

simulates the interactions between the HVAC system(s) and thermal zones [48]. It has also been validated through analytical [49,50], comparative [51–53], and executable tests. The governing equations used in EnergyPlus simulations are not presented here but fully available in the EnergyPlus engineering reference guide [54].

The stadium model (Figure 6) having an approximately equivalent interior volume of 1.1935×10^6 m^3 to that of the CFD stadium model of 1.1938×10^6 m^3 was developed using SketchUp [55] and then exported into EnergyPlus 9.3. The future weather file of 2022 used in EnergyPlus simulations was produced from the climate modeling program Meteonorm 7 [56,57] based on Doha international airport weather station data and the Intergovernmental Panel on Climate Change (IPCC) A1B emission scenario in the fourth assessment report (AR4) [58]. Meteonorm is a comprehensive meteorological program that provides the current and future weather data at most of the locations in the world in a variety of weather file formats [56]. Besides, the material used for the stadium and the ground follow the same settings as that defined in Fluent. The infiltration flow rates at each opening defined in EnergyPlus were coupled with those calculated based on CFD simulations, as presented in Table 4. To simplify the modeling of the HVAC system of air curtains and roof cooling, the native objects of HVAC templates were employed. In this case, a one-zone variable air volume (VAV) system was used to represent the system of air curtains and roof cooling due to the capability of adjusting the supply airflow rate for each air curtain or roof cooling supply slot. In addition to the air system, the chiller plant was also developed in the EnergyPlus model to provide cooling to the air system. The total supply airflow rate and supply air temperature for each cooling scenario, as listed in Table 4, were used for the VAV system. The thermostat cooling setpoint was set to 22.5 °C, the approximate median of the upper and lower thresholds of the FIFA comfort temperature range [4]. Moreover, the actual match schedules of the 2022 World Cup [59] were used to create the system operation schedules in order to predict the total energy consumption and the average energy consumption per match under the real match schedules. The duration of a match was assumed as 3 h, including a one-hour precooling before the match. It should be noted that the overtime for any matches at the knock-out stage was not considered in the energy consumption estimation.

Table 4. EnergyPlus building and HVAC model parameter settings.

Scenario	Total Supply Flow Rate (m^3/s)	Supply Temperature (°C)	Thermostat Cooling Setpoint (°C)	Infiltration Rate through All the Openings (m^3/s)
1	1643.2	20	22.5	2043.1
2	2081.9	20	22.5	2514.1
3	2520.5	20	22.5	2649.1
4	2137.6	20	22.5	2165.5
5	2137.6	15	22.5	2165.5
6	2137.6	10	22.5	2165.4

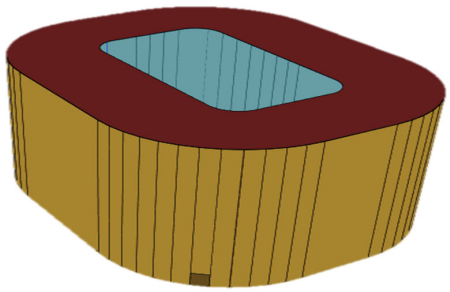

Figure 6. A simplified BES model of the stadium.

3. CFD Modeling Method Validation

The validation for the CFD modeling methods was implemented into two parts. The modeling of the stadium and surrounding environment was verified by the previous wind velocity measurements [13], and the modeling method of air curtains and roof cooling supply slot was validated by the experimental results from [30].

3.1. Validation for Stadium and Surrounding Buildings Modeling

The mean wind velocity at the stadium entrances was obtained from the wind conditions simulation under the wind direction of $\varphi = 350^\circ$ and compared with the wind velocity measurements from [13]. The normal velocity magnitude U/U_{ref} for each entrance was calculated from both results and plotted in a graph with error lines (Figure 7). The details of the results from the two methods and the errors between them were presented in Table 5. The deviations between the field measurements and CFD results could be caused since the exact locations of on-site testing points were not provided by [13]. A small error in the locations of data points at each entrance from the field measurement positions can result in a substantial discrepancy in the wind velocity magnitudes between the CFD simulations and actual measurements. The deviations between the two methods indicate a good agreement in Table 5, and therefore the modeling method of the stadium and surrounding environment is validated and employed in this work.

Table 5. Wind velocity validation results for the CFD model in the wind direction of 350°.

Opening	CFD Mean Velocity U_{CFD} (m/s)	U_{CFD}/U_{ref}	Experimental Mean Velocity U_{exp} (m/s)	U_{exp}/U_{ref}	Relative Difference
Gate A	3.09	0.39	4.00	0.50	−0.23
Gate B	4.91	0.61	4.11	0.51	0.19
Gate C	2.13	0.27	2.91	0.36	−0.27
Gate D	3.32	0.42	2.63	0.33	0.26

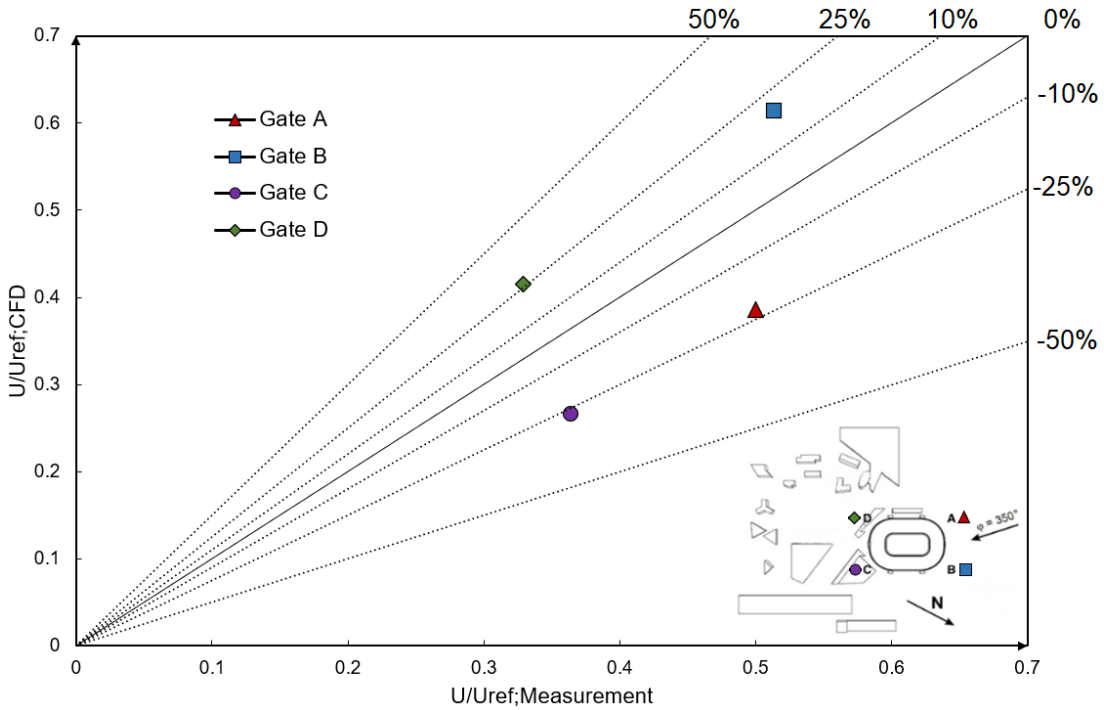

Figure 7. Wind velocity magnitude comparison between CFD simulations and on-site tests in the wind direction of 350°.

3.2. Air Curtain and Roof Cooling Supply Slots Modeling Method Validation

The air curtains and roof cooling supply are both developed as supply slots based on the existing work [30]. To verify the method used in modeling air curtains and roof cooling supply, a full-scale model of the experimental chamber [30], installed with an air curtain door and an exhaust fan, and its surroundings were developed in Fluent (Figure 8a). The depth (D_{ac}) and width (W_{ac}) of the air curtain supply slot were 0.0635 m and 0.61 m, and the width (W_d) and height (H_d) of the door were 0.61 m and 0.71 m, respectively. In addition, the length (L_c), width (W_c), and height (H_c) of the experimental chamber were 2.44 m, 2.44 m, and 1.3 m, respectively. Two sets of CFD simulations where a uniform supply speed of 13.75 m/s and 9.1 m/s were defined for the air curtain unit in each set of simulations, respectively. Attention needs to be paid to the fact that the uniform supply speed, rather than the actual supply speed profile of the experimental air curtain device, was employed in the present study since previous validation work [30] demonstrated that this simplification of the air curtain supply speed could still capture the flow characteristics of the air curtain device. The boundary conditions and the Fluent solver settings of the model were set the same as those presented in the previous work [29–31] and therefore not repeated in the present paper. Based on the two sets of CFD simulation results, the total flow rates through the door of the chamber Q under a variety of pressure differences across the door ΔP were calculated and compared with the experimental results and CFD simulation results from [30]. The measured data points from current simulation results and those data points and correlations from previous work are plotted in Figure 8b. The symbols of green triangles and magenta crosses represent the data points obtained from the current simulations under uniform supply speeds of 13.75 m/s and 9.1 m/s, respectively. As shown in Figure 8, the airflow rates from the present simulations under two sets of supply speeds are generally lower than those obtained from the experimental tests and estimated by the simulation correlations. However, the overall trend of the Q-DP relationships was still similar to those obtained from previous experimental tests and CFD simulations. Apart from this, the data points from the present simulations are close to those from the previous simulations where the uniform supply speeds were also applied. As a result, the modeling method of air curtains and roof cooling is validated and could capture the flow characteristics of air curtains and roof cooling supply slots.

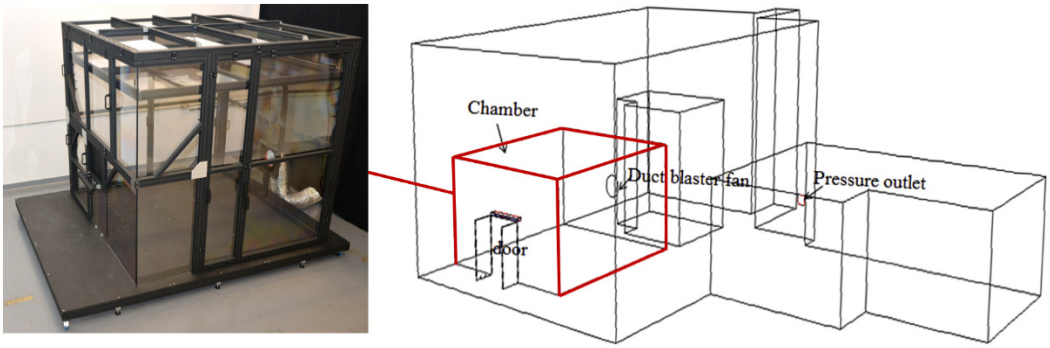

(**a**)

Figure 8. *Cont.*

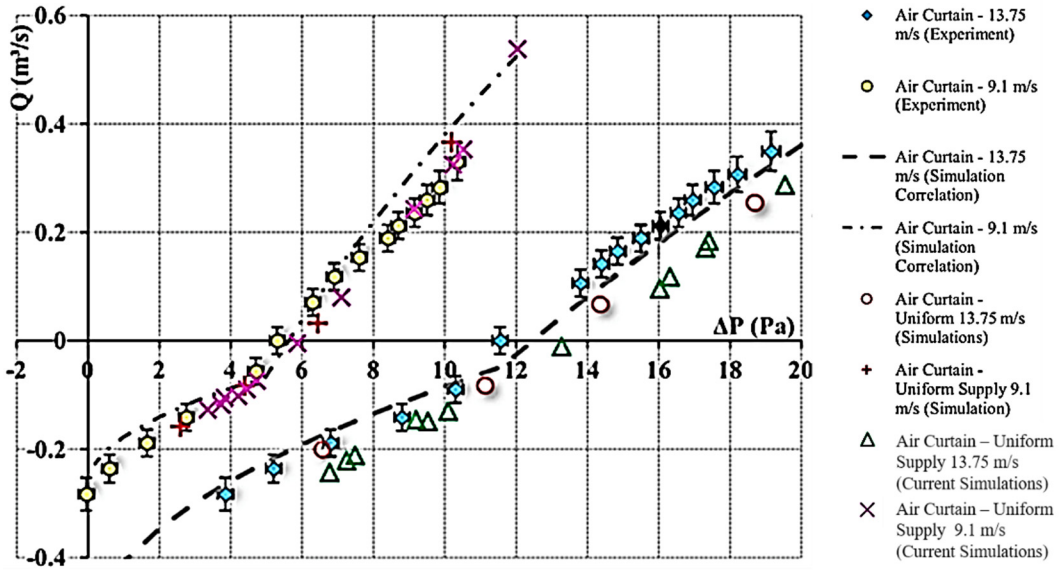

(**b**)

Figure 8. (**a**) experimental setup (**b**) Q–ΔP relationship comparisons among the CFD simulation results in this study and experimental and CFD simulation results from [30].

4. Results and Discussions

In this section, the solar radiation simulation results for providing boundary conditions of heat fluxes for the stadium model are presented in Section 4.1. The sensitivities of supply temperature and supply speed of air curtains and roof cooling supply slots on temperature and wind velocity of the spectator tiers and the pitch are explored in Sections 4.2 and 4.3. Six scenarios of the air curtain and roof cooling supply slots were proposed and are presented in Table 2 in Section 2.4. The thermal comfort indicators inside the stadium for the cooling scenarios in the sensitivity studies and the baseline stadium were also estimated based on the ASHRAE predicted mean vote (PMV) method (Standard 55–2017) [22]. Attention should be paid to the fact that the focus of the thermal comfort estimation was not on accurately predicting the thermal comfort levels inside the stadium but instead on using them as indicators to compare the thermal comfort levels among these scenarios and the baseline stadium. In Section 4.4, the baseline stadium performance was also assessed and compared with the stadium's cooling performance with air curtains and roof cooling. In addition, the total energy consumption of all the matches in the 2022 World Cup and the average energy consumption per match among these cooling scenarios were also estimated and compared in Section 4.5.

4.1. Solar Radiation Analysis Results

The solar radiation simulations were performed using the solar irradiance measurements for the proposed World Cup match kick-off times on the event opening day, i.e., 1 PM, 4 PM, 7 PM, and 10 PM (Doha time) [39]. According to the simulation results, the radiation heat fluxes emitted from the external and internal surfaces under each kick-off time were calculated and shown in Table 6. In addition, Figure 9 illustrates the contours of surface radiation heat flux on the ground at each time point. The highest radiative heat fluxes on these surfaces occurred at 1 PM compared with those at the other times. As a result, the radiation heat fluxes at this time were defined as the boundary conditions of heat flux for the simulations of temperature and wind velocity distributions for cooling scenarios and the baseline stadium.

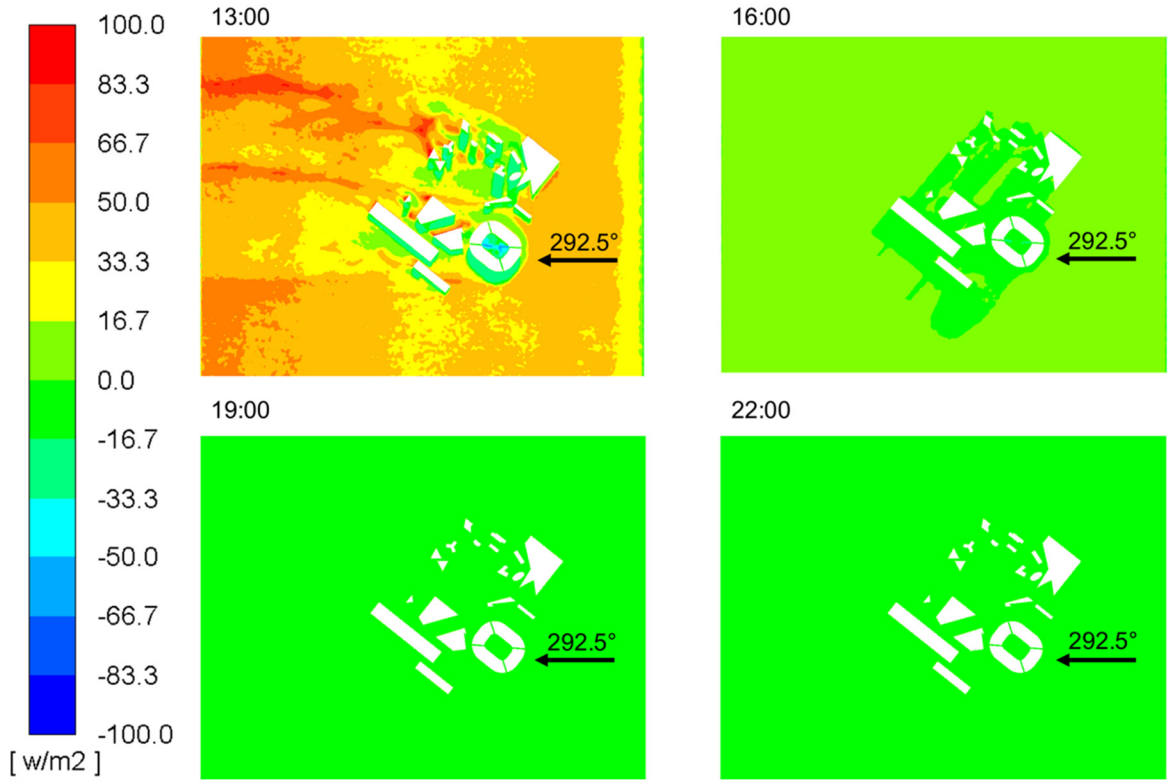

Figure 9. Radiation heat flux contours on the ground for the match kick-off times on the event opening day for the 2022 World Cup.

Table 6. Radiation heat fluxes for the ground, stadium, and surrounding buildings at kick-off times on the opening day of the event.

Radiative Heat Flux	13:00	16:00	19:00	22:00
Ground (W/m^2)	36.40	3.99	−0.42	−0.42
Stadium (W/m^2)	11.25	9.52	7.23	7.23
Surrounding (W/m^2)	3.10	4.91	2.95	2.95

4.2. Sensitivity Study of Supply Speed

Four scenarios of different supply speeds for the roof cooling and air curtain supply slots were studied in order to explore the impact of supply speed on the temperature and wind velocity distributions on spectator tiers and the pitch. Figure 10 includes the temperature and wind velocity contours of the cross-section of the stadium for these scenarios. The total pressure contours of the cross-section of the stadium for scenarios three and four are also illustrated in Figure 10. Figure 11 shows the temperature and wind velocity contours of the pitch for scenarios one to four. The thermal comfort levels, i.e., the PMV and the Predicted Percentage of Dissatisfied (PPD), on the upper and lower tiers, as well as the pitch for scenarios one to four, are presented in Table 7. Remarkably, scenario four presented the lowest temperature distributions in the range of 25.0–27.5 °C on the spectator tiers (Figure 10d) compared with the other three scenarios, mainly with 27.5–30.0 °C (Figure 10a–c), although the roof cooling supply velocity of 25 m/s of this scenario is lower than that of scenario three which was set to 30 m/s. According to the comparison of total pressure contours for scenarios three and four (Figure 10i,j), the high air supply velocity of scenario three resulted in negative pressure regions near the roof and positive pressure regions inside the stadium (Figure 10i), which contributed to the exfiltration of the cool jet air through the roof opening. However, for scenario four, it was observed that a majority of the regions inside the stadium were under negative pressure,

and positive pressure regions were observed near the roof (Figure 10j), which promotes the cool jet air entering into the lower levels of the stadium. This can also explain the temperature pattern for scenario three presented in Figure 10c, where the central region near the supply slot was cooled within 25–27.5 °C, but the remaining stadium bowl, including the majority of the spectator zone, had a higher temperature, up to 27.5–30.0 °C. The wind velocity contours (Figure 10e–h) showed that the air movement for each scenario is more active below one end of the roof than another end. This could be explained by the scouring effect of outside air entering the stadium from one end of the roof [60]. The most active air movement below one end of the roof (Figure 10g) was observed in scenario three due to it having the highest roof cooling supply velocity magnitude. Considering both parameters together using the ASHRAE PMV method [22], the PMV values for the upper spectator tiers are all within 1 for the four scenarios with low PPDs of 12% and 5% for scenarios one and two and scenarios three and four, which had overall 'Slightly warm' to 'Neutral' thermal sensation, respectively [22]. The PPDs for the lower tiers were also around 10% for scenarios two to four, but scenario one had a PPD of 38% on the lower tiers, which was still 'Slightly warm' [22] for the spectators.

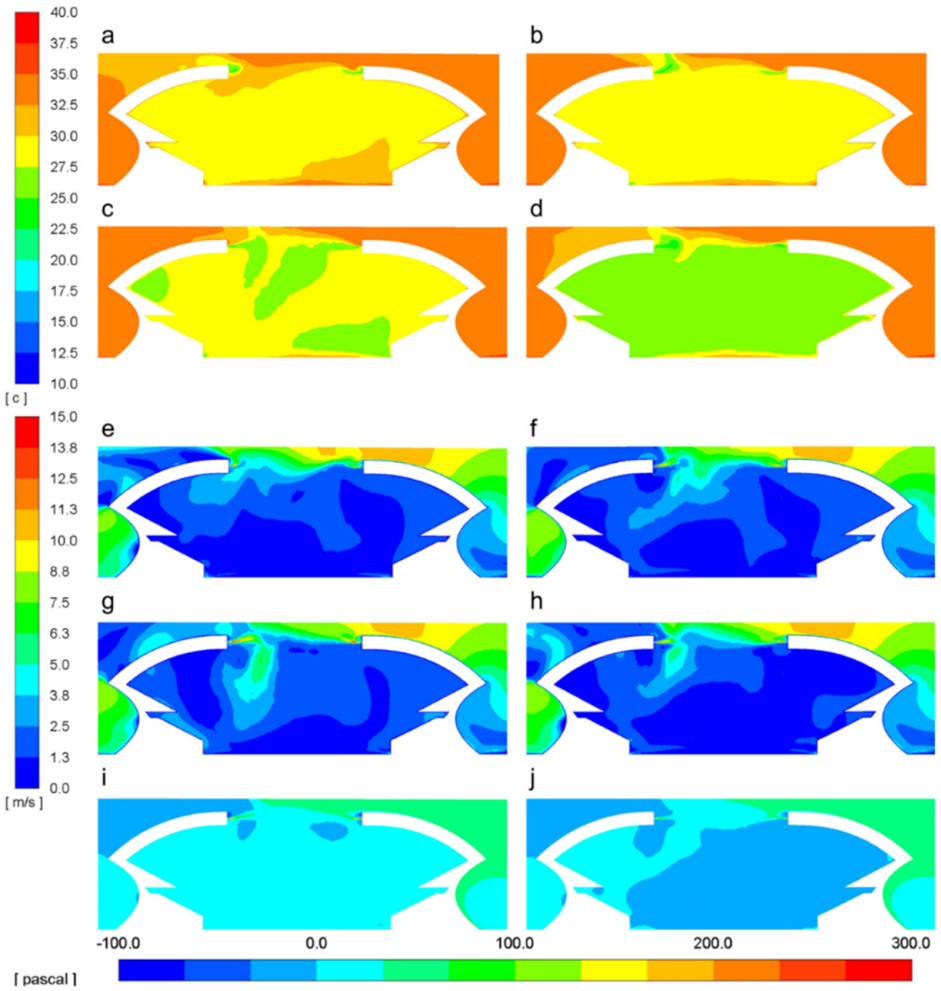

Figure 10. (**a**–**d**) Temperature contours of the cross-section of the stadium for scenarios one to four. (**e**–**h**) Wind velocity contours of the cross-section of the stadium for scenarios one to four. (**i**,**j**) Total pressure contours of the cross-section of the stadium for scenarios three to four.

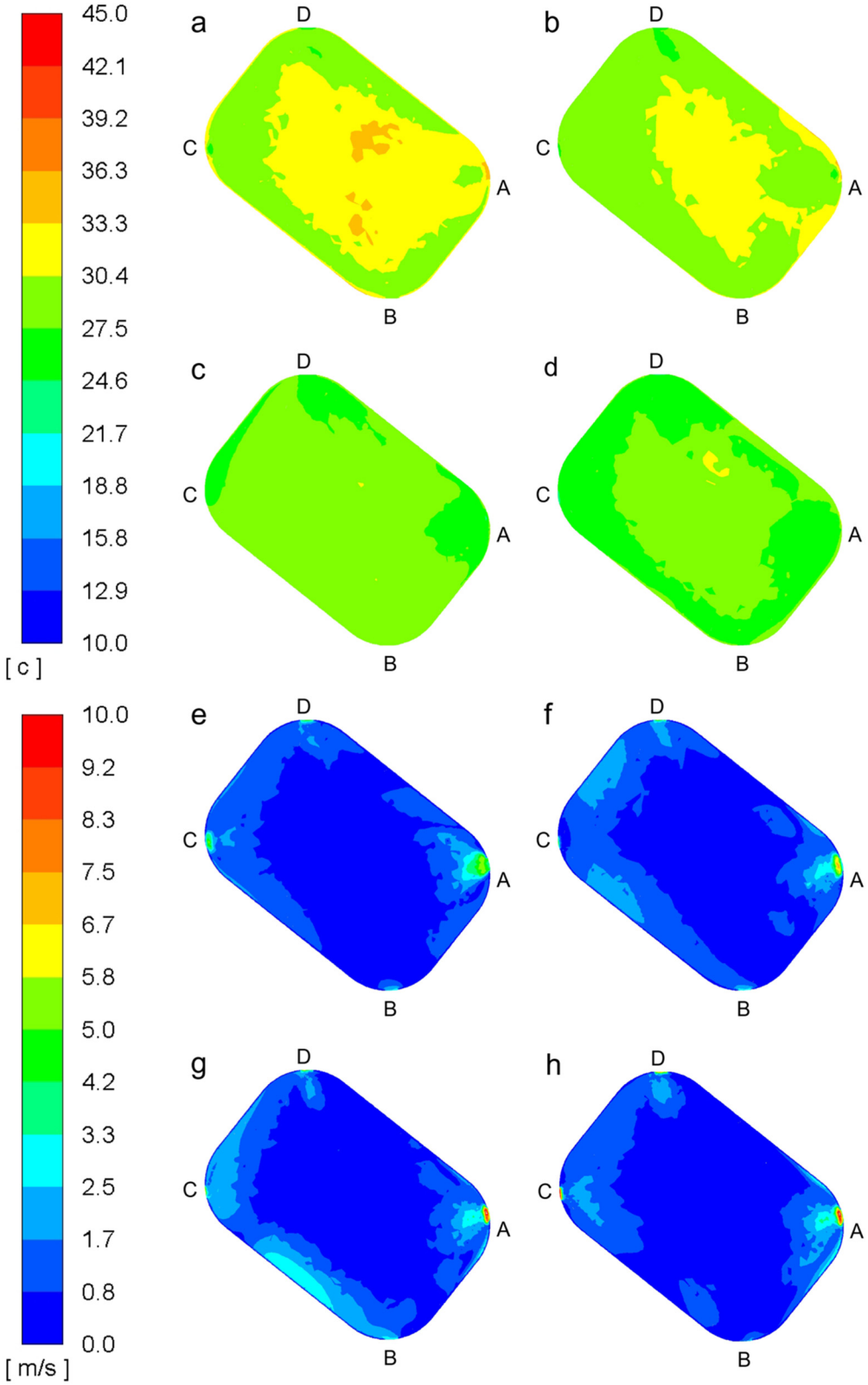

Figure 11. (**a**–**d**) Temperature contours of the pitch for scenarios one to four. (**e**–**h**) Wind velocity contours of the pitch for scenarios one to four.

Table 7. Thermal comfort indexes and energy consumption estimations.

Air Curtain and Roof Cooling Scenarios	Thermal Comfort Estimation (PMV/PPD)			Total Energy Consumption (MWh)	Energy Consumption per Match (MWh)
	Upper Tiers	Lower Tiers	Pitch		
Scenario one	0.59/12%	1.26/38%	4.11/100%	906.2	14.2
Scenario two	0.59/12%	0.59/12%	3.24/100%	1144.8	17.9
Scenario three	0.06/5%	0.27/6%	2.37/90%	1371.2	21.4
Scenario four	−0.03/5%	0.24/6%	1.98/76%	1161.1	18.1
Scenario five	−0.63/13%	−0.35/8%	1.40/45%	1406.5	22.0
Scenario six	−1.21/36%	−0.92/23%	0.90/22%	1631.4	25.5
Baseline	2.93/99%	2.74/97%	5.90/100%		

As for the pitch, the temperature distributions for scenarios three and four (Figure 11c,d) were significantly lower than those observed for scenarios one and two (Figure 11a,b). The regions near gate A had higher temperature distributions than the remaining pitch regions for scenarios one and two since gate A is in the prevailing wind direction and a high flow rate of outside air is pushed through gateway A by the prevailing wind, as observed in Figure 11e–h. Figure 12 illustrates the air curtain performance at gate A for these scenarios. Based on the simulated wind conditions, the air curtains with 20 m/s for scenarios three and four showed better performances in blocking the penetration of outside hot air of 34.2 °C and 5 m/s at the middle level of gate A than the air curtains with 10 m/s and 15 m/s for the scenarios one and two, respectively. However, the operational conditions of the air curtain at gate A for the four scenarios are all under the outflow break-through conditions, which means that the air curtain performance would still require being enhanced. This limitation can be improved by adjusting the supply speed and the supply angle of the air curtain, which will be covered in an ongoing study by the authors. In terms of thermal comfort for players, all four scenarios performed poorly, with the lowest PMV and PPD of 1.98 and 76% among all these scenarios. The PMVs on the pitch for scenarios one and two could be even higher than three, which were hot for players.

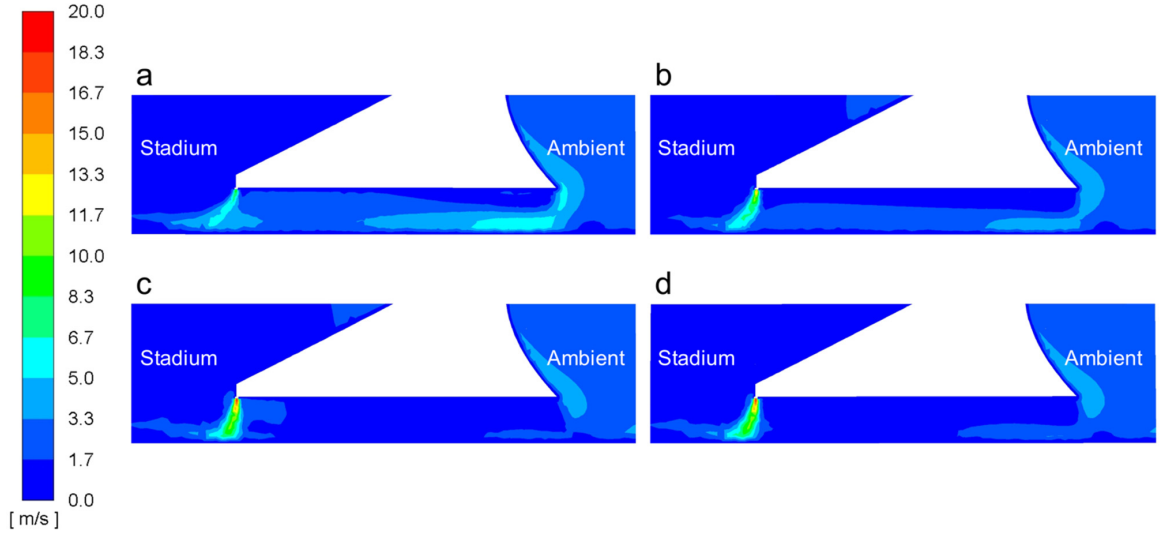

Figure 12. (**a**–**d**) Wind velocity contours of gateway A for scenarios one to four.

4.3. Sensitivity Study of Supply Temperature

In addition to the sensitivity analysis of supply speed of air curtain and roof cooling supply slots, the effect of supply temperature on the cooling performance of the stadium is explored. Scenarios four to six, which had different supply temperatures of 20 °C, 15 °C,

and 10 °C, but the same supply speeds at gates and roof, were included in this study. The temperature distributions of the cross-section of the stadium and pitch for these scenarios are shown in Figure 13. The cooling performance improved gradually with the decrease in supply temperature from 20 °C to 15 °C and to 10 °C for scenarios four to six. Scenario four showed temperature distributions of 25–27.5 °C on the spectator tiers, which were still higher than the FIFA's comfort temperature range of 20–25.5 °C. However, scenarios five and six could maintain the spectator tiers within this comfort temperature range. Based on the estimation of thermal comfort indexes on the spectator tiers, the PPDs for both the upper and lower tiers were around 10% for scenarios four and five, which were 'Neutral' to 'Slightly cool' [22] for the spectators, but the PMVs dropped below −1 and were nearly −1 for the upper and lower tiers, respectively, for scenario six, which were both 'Slightly cool' [22].

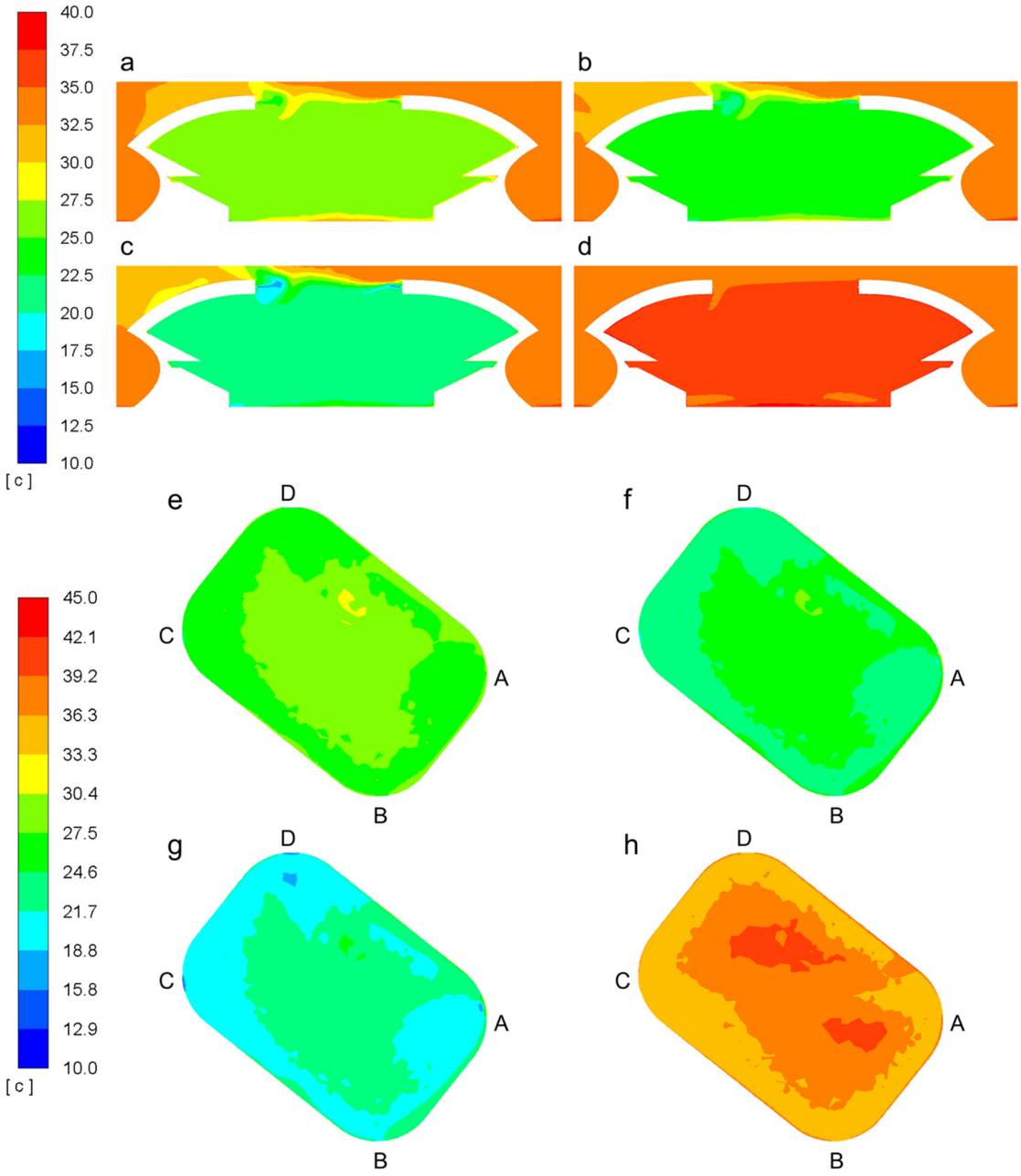

Figure 13. (**a**–**d**) Temperature contours of the cross-section of the stadium for scenarios four to six and for the baseline stadium. (**e**–**h**) Temperature contours of the pitch for scenarios four to six and for the baseline stadium.

With regards to the pitch, the outer perimeter of the pitch had a lower temperature than the central region of the pitch for all three scenarios. It could be attributed to the limited cooling distance of the supply of air from the air curtains. The temperature around the outer perimeter is on average 3 °C lower than that of the central region. Remarkably, the temperature distributions for scenario six could be maintained within 18.8–24.6 °C with the supply temperature decreasing to 10 °C. As for the thermal comfort of players, completely different from that of spectators, the PMVs for the pitch were still over 1 for scenarios four and five with the corresponding PPDs of 76% and 45%, respectively, which were 'Warm' to 'Slightly warm' [22]. However, scenario six could present a significantly more comfortable thermal environment on the pitch with only 22% of PPD.

4.4. Comparison between Baseline Stadium Performance and Cooling Scenario Performance

The temperature distributions of the stadium cross-section and the pitch for the baseline stadium are presented in Figure 13d,h. Both the thermal performances of spectator tiers and pitch were extremely hot. The temperature of the spectator tiers for the baseline stadium was 35.0–37.5 °C, and that of the pitch was 33.3–36.3 °C for the outer perimeter of the pitch and 36.3–42.1 °C for the central region of the pitch. According to the thermal comfort evaluation, the PMVs for the upper and lower tiers are close to 3, and that for the pitch approximately reaches 6, which is extremely hot for both spectators and players. Thus, the baseline thermal performance is significantly poor. By comparing scenario six, which was the coolest scenario among all the scenarios, with the baseline stadium, the thermal performances of both the spectator tiers and the pitch were substantially enhanced. The average reductions in temperature on the spectator tiers and on the pitch were 15 °C and 14.6 °C, respectively. The reductions in PPDs for the upper and lower tiers as well as the pitch were 63%, 74%, and 78%.

4.5. EnergyPlus Energy Consumption Estimations for Cooling Scenarios

The total energy consumptions of all the 64 World Cup matches and average energy consumptions per match for the cooling scenarios were estimated using EnergyPlus simulations and are presented in Table 7 in Section 4.2. Overall, the total and average energy consumption rose with the increase in the total supply airflow rate of air curtains and roof cooling and the decrease in their supply air temperature. It is also observed that the average energy consumption of 21.4 MWh of scenario three, which had the largest total supply airflow rate, was similar to the 22.0 MWh of scenario five. However, the cooling performance of these two scenarios on the cross-section and the pitch of the stadium is significantly different. The temperatures on the cross-section of the stadium and on the pitch for scenario five were 2.5–5 °C and 2.9–5.8 °C lower than those for scenario three, respectively. Moreover, compared with the energy consumption of air conditioning system per match of 22.8 MWh for one of the stadiums in 2010 South Africa World Cup (highest outdoor temperature of 24.4 °C) [61] and that of 42.0 MWh for the 2006 Germany World Cup (highest outdoor temperature of 34.5 °C) [2], scenario six, the lowest temperature scenario, would consume an average energy consumption of 25.5 MWh (highest design outdoor temperature of 34.2 °C). Apart from this, in comparison with that of 54.0 MWh of the lowest temperature scenario for an integrated cooling jet and air curtain system proposed for the 2022 Qatar World Cup in previous work [23], the average energy consumption of scenario six for the system of air curtain gates and roof cooling in this study was reduced by 52.8%.

5. Conclusions and Future Works

This study evaluated the thermal and wind conditions for stadiums equipped with roof cooling supply slots and air curtain gates in hot climates and to explore the effect of the supply speed and the supply temperature of air curtain and roof cooling supply slots on the cooling performance of stadiums in hot climates. In addition, this study estimated the total energy consumption required for all the matches of the 2022 World Cup as well as the

average energy consumption per match and compared the energy consumption estimations with those consumed by the mechanical cooling system proposed in the previous work and the actual energy consumptions consumed by the air-conditioning systems in the previous World Cups. The stadium model, with its surrounding environment, was created at full scale and validated based on previous work. The air curtain and roof cooling supply were also modeled in the stadium model and validated by the experimental and CFD simulation results of previous studies. In addition, separate solar radiation simulations, apart from simulations evaluating the thermal and wind environment for stadiums, were carried out for the baseline stadium without air curtains and roof cooling in order to estimate the radiation heat fluxes on the external and internal surfaces. The estimated radiative heat fluxes were input as boundary conditions of heat flux for simulating the thermal and wind conditions of cooling scenarios and the baseline stadium. Six cooling scenarios investigating the sensitivities of supply speed and supply temperature of air curtains and roof cooling were proposed. The thermal comfort indexes inside the stadium were also predicted based on the ASHRAE PMV method (Standard 55-2017) and used in the comparison among these scenarios and the baseline stadium.

Based on the simulated conditions, the sensitivity study of different supply speeds for air curtain and roof cooling revealed that scenario four had the lowest temperature distributions in the range of 25.0–27.5 °C on the spectator tiers among the scenarios one to four, although the roof cooling supply velocity of 25 m/s for scenario four was lower than that of scenario three. This could be explained by the local negative pressure regions near the roof and the positive pressure regions inside the stadium caused by the high supply air velocity of scenario three, which contributes to the exfiltration of the cool jet air through the roof. However, for scenario four, it was observed that a majority of the regions inside the stadium were under negative pressure, and positive pressure regions were observed near the roof, which would promote cool jet air entering the stadium. Apart from this, it was remarkable that the air curtains with 20 m/s for scenarios three and four were effective in blocking the infiltration of outside hot air of 34.2 °C and 5 m/s. However, the lowest PMV and PPD of these scenarios could still reach 1.98 and 76%, which is hot for players.

Scenarios four to six with different supply temperatures of 20 °C, 15 °C, and 10 °C but the same supply speeds were studied to evaluate the effect of supply temperature on the cooling performance of the stadium. The results show that scenarios five and six can provide comfortable temperatures in the tiers with 'Neutral' to 'Slightly cool' sensation. In addition to the tiers, scenario six could provide a significantly more comfortable thermal environment on the pitch with only 22% of PPD. Moreover, the temperature around the outer perimeter is, on average, 3 °C lower than that of the central region due to the limited cooling distance of the supply air from air curtains. Compared with the performance of the baseline stadium, the thermal conditions of the stadium would be significantly improved. The average reductions in temperature on the spectator tiers and on the pitch could reach 15 °C and 14.6 °C. The reductions in PPDs for the upper and lower tiers as well as the pitch are 63%, 74%, and 78%. In terms of the estimated energy consumptions, scenario six would consume energy at 25.5 MWh per match (highest design outdoor temperature of 34.2 °C) compared with 22.8 MWh for one of the stadiums in the 2010 South Africa World Cup (highest outdoor temperature of 24.4 °C) and 42.0 MWh for the 2006 Germany World Cup (highest outdoor temperature of 34.5 °C). In addition, the energy consumption per match of scenario six would be 52.8% lower than that of the coolest scenario for an integrated cooling jet and air curtain system proposed for the 2022 Qatar World Cup in the previous study.

Future work is recommended to focus on exploring the influence of supply angle on the performances of air curtain gates and roof cooling supply slots. In addition, the roof cooling supply slot can be controlled according to the actual outdoor air sealing performances on the divisions of the roof opening. Besides, the field testing of air curtains and roof cooling slots in the actual World Cup stadiums under the hot climate is also worth carrying out.

Author Contributions: Conceptualization, F.Z. and J.K.C.; methodology, F.Z. and J.K.C.; software, F.Z.; validation, F.Z.; formal analysis, F.Z.; investigation, F.Z.; resources, J.K.C.; writing—original draft preparation, F.Z.; writing—review and editing, J.K.C. and H.N.C.; visualization, F.Z.; supervision, J.K.C.; project administration, J.K.C.; funding acquisition, J.K.C. All authors have read and agreed to the published version of the manuscript.

Funding: This research received no external funding.

Acknowledgments: The authors would like to thank the support of the Department of Architecture and Built Environment at the University of Nottingham for providing the facility for carrying out the modeling and simulations.

Conflicts of Interest: The authors declare no conflict of interest.

References

1. Talavera, A.M.; Al-Ghamdi, S.G.; Koç, M. Sustainability in Mega-Events: Beyond Qatar. *Sustainability* **2019**, *11*, 6407. [CrossRef]
2. FIFA.com. Available online: https://www.fifa.com/mm/document/afsocial/environment/01/57/12/66/2006fwcgreengoallegacyreport_en.pdf (accessed on 26 November 2018).
3. Saffouri, F.; Bayram, I.S.; Koc, M. Quantifying the Cost of Cooling in Qatar. In Proceedings of the 2017 9th IEEE-GCC Conference and Exhibition (GCCCE), Manama, Bahrain, 8–11 May 2017; pp. 1–9.
4. FIFA.com. Available online: https://www.fifa.com/mm/document/tournament/competition/01/37/17/76/stadiumbook2010_buch.pdf (accessed on 26 November 2018).
5. FIFA.com. Available online: https://www.fifa.com/worldcup/news/2022-fifa-world-cup-to-be-played-in-november-december-2568172 (accessed on 26 November 2018).
6. The American Society of Heating, Refrigeration and Air-conditioning Engineers (ASHRAE). *ASHRAE Weather Data 2017*; ASHRAE: Atlanta, GA, USA, 2017; p. 929.
7. Bagasi, A.A.; Calautit, J.K.; Karban, A.S. Evaluation of the Integration of the Traditional Architectural Element Mashrabiya into the Ventilation Strategy for Buildings in Hot Climates. *Energies* **2021**, *14*, 530. [CrossRef]
8. Ghoulem, M.; El Moueddeb, K.; Nehdi, E.; Zhong, F.; Calautit, J. Design of a Passive Downdraught Evaporative Cooling Windcatcher (PDEC-WC) System for Greenhouses in Hot Climates. *Energies* **2020**, *13*, 2934. [CrossRef]
9. Soleimani, Z.; Calautit, J.K.; Hughes, B.R. Computational Analysis of Natural Ventilation Flows in Geodesic Dome Building in Hot Climates. *Computation* **2016**, *4*, 31. [CrossRef]
10. Calautit, J.K.; O'Connor, D.; Sofotasiou, P.; Hughes, B.R. CFD Simulation and Optimisa-tion of a Low Energy Ventilation and Cooling System. *Computation* **2015**, *3*, 128–149. [CrossRef]
11. Nejat, P.; Jomehzadeh, F.; Hussen, H.M.; Calautit, J.K.; Majid, M.Z.A. Application of Wind as a Renewable Energy Source for Passive Cooling through Windcatchers Integrated with Wing Walls. *Energies* **2018**, *11*, 2536. [CrossRef]
12. Jiang, Z.; Gao, W. Impact of Enclosure Boundary Patterns and Lift-Up Design on Opti-mization of Summer Pedestrian Wind Environment in High-Density Residential Districts. *Energies* **2021**, *14*, 3199. [CrossRef]
13. Van Hooff, T.; Blocken, B. Coupled Urban Wind Flow and Indoor Natural Ventilation Modelling on a High-resolution Grid: A Case Study for the Amsterdam Arena Stadium. *Environ. Model. Softw.* **2010**, *25*, 51–65. [CrossRef]
14. Van Hooff, T.; Blocken, B. On the Effect of Wind Direction and Urban Surroundings on Natural Ventilation of a Large Semi-enclosed Stadium. *Comput. Fluid.* **2010**, *39*, 1146–1155. [CrossRef]
15. Van Hooff, T.; Blocken, B. Full-scale Measurements of Indoor Environmental Conditions and Natural Ventilation in a Large Semi-enclosed Stadium: Possibilities and Limitations for CFD Validation. *J. Wind Eng. Ind. Aerodyn.* **2012**, *104–106*, 330–341. [CrossRef]
16. Sofotasiou, P. Aerodynamic Optimization of Sports Stadiums towards Wind Comfort. Ph.D. Thesis, University of Sheffield, Sheffield, UK, 2017.
17. Sofotasiou, P.; Hughes, B.R.; Calautit, J.K. Qatar 2022: Facing the FIFA World Cup Climatic and Legacy Challenges. *Sustain. Cities Soc.* **2015**, *14*, 16–30. [CrossRef]
18. Losi, G.; Bonzanini, A.; Aquino, A.; Poesio, P. Analysis of thermal comfort in a football stadium designed for hot and humid climates by CFD. *J. Build. Eng.* **2021**, *33*, 101599. [CrossRef]
19. Ghani, S.; ElBialy, E.A.; Bakochristou, F.; Gamaledin, S.M.A.; Rashwan, M.M.; Hughes, B. Thermal performance of stadium's Field of Play in hot climates. *Energy Build.* **2017**, *139*, 702–718. [CrossRef]
20. Khalil, E.E.; Ashmawy, M.E. The Challenge of Cooling Football Stadiums in Qatar. *CIBSE J.* **2017**. Available online: https://www.cibsejournal.com/technical/sporting-success-a-study-of-air-conditioning-stadiums-in-qatar/ (accessed on 18 March 2019).
21. Zhong, F.; Calautit, J.K.; Hughes, B.R. Analysis of the influence of cooling jets on the wind and thermal environment in football stadiums in hot climates. *Build. Serv. Eng. Res. Technol.* **2019**, *41*, 561–585. [CrossRef]
22. The American Society of Heating, Refrigeration and Air-conditioning Engineers (ASHRAE). *ASHRAE Handbook Fundamentals*; ASHRAE: Atlanta, GA, USA, 2017.

23. Zhong, F.; Calautit, J. An Integrated Cooling Jet and Air Curtain System for Stadiums in Hot Climates. *Atmosphere* **2020**, *11*, 546. [CrossRef]
24. Giráldez, H.; Perez-Segarra, C.-D.; Oliet, C.; Oliva, A. Heat and moisture insulation by means of air curtains: Application to refrigerated chambers. *Int. J. Refrig.* **2016**, *68*, 1–14. [CrossRef]
25. Foster, A.; Swain, M.; Barrett, R.; D'Agaro, P.; Ketteringham, L.; James, S. Three-dimensional effects of an air curtain used to restrict cold room infiltration. *Appl. Math. Model.* **2007**, *31*, 1109–1123. [CrossRef]
26. Lecaros, M.; Elicer-Cortés, J.; Fuentes, A.; Felis, F. On the ability of twin jets air curtains to confine heat and mass inside tunnels. *Int. Commun. Heat Mass Transf.* **2010**, *37*, 970–977. [CrossRef]
27. Wang, B.; Yu, J.; Ye, H.; Liu, Y.; Guo, H.; Tian, L. Study on Present Situation and Opti-mization Strategy of Infiltration Air in a Train Station in Winter. *Proc. Eng.* **2017**, *205*, 2517–2523. [CrossRef]
28. Hayes, F.C.; Stoecker, W.F. Design Data for Air Curtains. *Trans. ASHRAE* **1969**, *75*, 168–180.
29. Wang, L.; Zhong, Z. An approach to determine infiltration characteristics of building entrance equipped with air curtains. *Energy Build.* **2014**, *75*, 312–320. [CrossRef]
30. Goubran, S.; Qi, D.; Saleh, W.F.; Wang, L.; Zmeureanu, R. Experimental study on the flow characteristics of air curtains at building entrances. *Build. Environ.* **2016**, *105*, 225–235. [CrossRef]
31. Qi, D.; Goubran, S.; Wang, L.; Zmeureanu, R. Parametric study of air curtain door aerodynamics performance based on experiments and numerical simulations. *Build. Environ.* **2018**, *129*, 65–73. [CrossRef]
32. Blocken, B.; Persoon, J. Pedestrian wind comfort around a large football stadium in an urban environment: CFD simulation, validation and application of the new Dutch wind nuisance standard. *J. Wind. Eng. Ind. Aerodyn.* **2009**, *97*, 255–270. [CrossRef]
33. Franke, J.; Hellsten, A.; Schlünzen, H.; Carissimo, B. *Best Practice Guideline for the CFD Simulation of Flows in the Urban Environment*; COST Office: Brussels, Belgium, 2007. Available online: https://www.semanticscholar.org/paper/BEST-PRACTICE-GUIDELINE-FOR-THE-CFD-SIMULATION-OF-Franke-Hellsten/bc39516aba1e74f7d8ed7391b4ff9e5a9ceeecf2 (accessed on 2 May 2019).
34. Bartzis, J.G.; Vlachogiannis, D.; Sfetsos, A. Thematic area 5: Best practice advice for en-vironmental flows. *QNET-CFD Netw. Newsl.* **2004**, *2*, 34–39.
35. Mohammadi, M.; Calautit, J.K. Numerical Investigation of the Wind and Thermal Con-ditions in Sky Gardens in High-Rise Buildings. *Energies* **2019**, *12*, 1380. [CrossRef]
36. Mohammadi, M.; Tien, P.; Calautit, J.K. Influence of Wind Buffers on the Aero-Thermal Performance of Skygardens. *Fluids* **2020**, *5*, 160. [CrossRef]
37. Nejat, P.; Hussen, H.M.; Fadli, F.; Chaudhry, H.N.; Calautit, J.; Jomehzadeh, F. Indoor Environmental Quality (IEQ) Analysis of a Two-Sided Windcatcher Integrated with An-ti-Short-Circuit Device for Low Wind Conditions. *Processes* **2020**, *8*, 840. [CrossRef]
38. Chaudhry, H.N.; Calautit, J.K.; Hughes, B.R.; Sim, L.F. CFD and Experimental Study on the Effect of Progressive Heating on Fluid Flow inside a Thermal Wind Tunnel. *Computation* **2015**, *3*, 509–527. [CrossRef]
39. Kick-off Times Confirmed for 2022 FIFA World Cup in Qatar. Available online: https://punditarena.com/football/mcorry/kick-off-qatar-world-cup-fifa/ (accessed on 12 January 2020).
40. Perez-Astudillo, D.; Bachour, D. DNI, GHI and DHI Ground Measurements in Doha, Qatar. *Energy Proc.* **2014**, *49*, 2398–2404. [CrossRef]
41. Weather Online. Available online: https://www.weatheronline.co.uk/weather/maps/city (accessed on 18 March 2019).
42. Blumberg, D.; Greeley, R. Field studies of aerodynamic roughness length. *J. Arid. Environ.* **1993**, *25*, 39–48. [CrossRef]
43. Launder, B.; Spalding, D. The numerical computation of turbulent flows. *Comput. Methods Appl. Mech. Eng.* **1974**, *3*, 269–289. [CrossRef]
44. Cebeci, T.; Bradshaw, P. *Momentum Transfer in Boundary Layers*; Hemisphere Publications Co.: Washington, DC, USA, 1977.
45. Incropera, F.P. *Introduction to Heat Transfer*, 5th ed.; John Wiley & Sons: Franklin Township, NJ, USA, 2007.
46. Mochida, A.; Tominaga, Y.; Murakami, S.; Yoshie, R.; Ishihara, T.; Ooka, R. Comparison of various k-ε models and DSM applied to flow around a high-rise building—Report on AIJ cooperative project for CFD prediction of wind environment. *Wind. Struct. Int. J.* **2002**, *5*, 227–244. [CrossRef]
47. Franke, J.; Hirsch, C.; Jensen, A.G.; Krüs, H.W.; Schatzmann, M.; Westbury, P.S.; Miles, S.D.; Wisse, J.A.; Wright, N.G. Recommendations on the use of CFD in wind engineering. In *COST Action C14*; COST Office: Brussels, Belgium, 2004.
48. U.S. Department of Energy (DOE). *EnergyPlus Version 9.3 Getting Started*; DOE: Washington, DC, USA, 2020.
49. ASHRAE. *ASHRAE RP-865 Development of Accuracy Tests for Mechanical System Simulations*; ASHRAE: Atlanta, GA, USA, 2002.
50. Rees, S.J.; Xiao, D.; Spitler, J.D. An Analytical Verification Test Suite for Building Fabric Models in Whole Building Energy Simulation Programs. *Trans. ASHRAE* **2002**, *108*, 30–41.
51. American National Standards Institute (ANSI); ASHRAE. *ANSI/ASHRAE Standard 140–2011 Standard Method of Test for The Evaluation of Building Energy Analysis Computer Programs*; ASHRAE: Atlanta, GA, USA, 2011.
52. Judkoff, R.; Neymark, J. *International Energy Agency Building Energy Simulation Test (BESTEST) and Diagnostic Method*; National Renewable Energy Lab: Golden, CO, USA, 1995.
53. DOE. EnergyPlus HVAC Component Comparative Tests. Available online: https://energyplus.net/sites/all/modules/custom/nrel_custom/eplus_files/current_testing_reports/HVACComponent-8.3.0-b45b06b780.pdf (accessed on 1 December 2020).
54. DOE. *EnergyPlus Version 9.3 Engineering Reference*; DOE: Washington, DC, USA, 2020.

55. Trimble. SketchUp. Available online: https://www.sketchup.com (accessed on 17 December 2020).
56. Remund, J.; Müller, S.; Kunz, S.; Schilter, C. *Meteonorm Handbook Part I: Software*; METE-OTEST: Bern, Switzerland, 2012.
57. Remund, J.; Müller, S.; Kunz, S.; Schilter, C. *Meteonorm Handbook Part II: Theory*; METE-OTEST: Bern, Switzerland, 2012.
58. Intergovernmental Panel on Climate Change (IPCC). 2007: Global Climate Projections. In *Climate Change 2007: The Physical Science Basis*; Cambridge University Press: Cambridge, UK, 2007.
59. FIFA. Available online: https://www.fifa.com/worldcup/news/fifa-world-cuptm-match-schedule-confirmed-hosts-qatar-to-kick-off-2022-tournamen (accessed on 11 December 2020).
60. Simpson, M. Computerised design of stadiums. In *Stadium and Arena Design*; Institution of Civil Engineers (ICE): London, UK, 2015; pp. 119–132.
61. Department of Environment, Forestry and Fisheries. Chapter 4: Energy. In *World Cup Legacy Report*; Department of Environment, Forestry and Fisheries: Cape Town, South Africa, 2011.